RSC Advances

ROYAL SOCIETY OF CHEMISTRY

www.rsc.org/advances

The optimal adsorption pattern of hydroxamate onto TiO_2 anatase surface has been theoretically determined

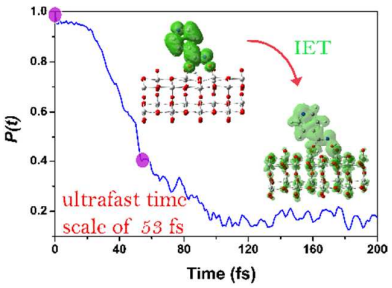

Journal Name RSCPublishing

COMMUNICATION

Theoretical investigation of the adsorption, IR, and electron injection of hydroxamate anchor at the TiO_2 anatase (1 0 1) surface

Cite this: DOI: 10.1039/x0xx00000x

Received 00th January 2012,
Accepted 00th January 2012

DOI: 10.1039/x0xx00000x

www.rsc.org/

Wei Li,[a] Luis G. C. Rego,[b] Fu-Quan Bai,[*a] Chui-Peng Kong,[a] and Hong-Xing Zhang[*a]

The adsorption of hydroxamate onto TiO_2 anatase surface has been theoretically determined. We find that doubly deprotonated configuration is the optimal adsorption mode in terms of energetic and dynamical stability, which is demonstrated by vibrational spectrum analysis. This configuration can also undergo the ultrafast electron transfer event, with a time-scale of 53 fs.

Among renewable energy solutions, dye-sensitized solar cells (DSSC), have attracted intensive attention as the alternative for light-to-electricity conversion.[1] In DSSC system, the light energy is harvested by dye molecules grafted onto the nanocrystalline semiconductor through the anchor group. The photo-excited electrons are then transferred, resulting in electron-hole separation at the dye/semiconductor interface. The highest conversion efficiency for DSSC has reached 12.3% in experiment,[2] but it is still low for large-scale implantation. The appeals for investigating the structure and electronic interaction of adsorbate/substrate interface are urgent, as they are crucial in determining the time-scale of electron injection following the photo-excitation of dye. In the meanwhile, the dye must anchor strongly onto the substrate to ensure the long-term stability of the cell. Carboxylic acid is the commonly used anchor group, as it appears to give good electronic coupling across the dye/TiO_2 interface. However, the dye bearing carboxylic acid anchor may be affected by the limited stability in the presence of water and highly oxidizing conditions, which make it unsuitable for use in an artificial photosynthetic cell. Some other groups, i.e., phosphonic acid,[3] biscarbodithiolic acid,[4] and hydroxamic acid[5] have also been reported to date. Among these, hydroxamic acid stands out for its long-term stability and efficient electron injection. Although there are a number of experimental works concerning the hydroxamate anchor,[5] however, the preferred configuration of hydroxamate adsorbed on the titanium dioxide surface has not been unambiguously determined yet.

In this work we systematically study the adsorption configurations of hydroxamic anchor on the TiO_2 anatase (1 0 1) surface. The geometry optimization was performed with the Vienna ab initio simulation package (VASP),[6] using the generalized gradient approximation (GGA) of Perdewe-Wang 91 (PW91) exchange-correlation functional[7]. The bulk anatase TiO_2 was relaxed with a k-point of (5, 5, 2) and an energy cutoff of 400 eV. A slab comprised of two layers (2 × 4) of titanium and oxygen atoms was used (Fig. S1). This set of parameters gives a force convergence within 0.01 eV/Å. We choose the hydroxamic acid functionalized with pyridine as the anchor model, since it provides an important stepping-stone from detailed studies of small molecules on metal oxide surfaces to investigate the full DSSC system. Molecular dynamics simulations of various adsorbate/TiO_2 systems were also performed with VASP. In this calculation a time step of 1 fs is used, producing the total time of 4 ps.

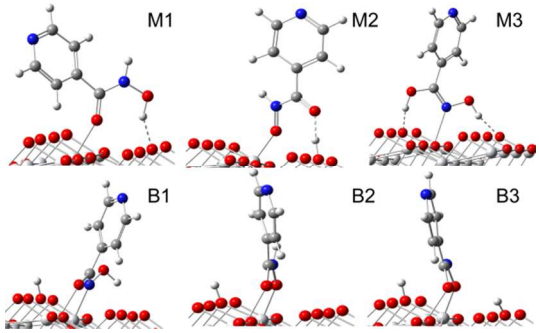

Fig. 1. The different adsorption configurations of the hydroxamate anchor.

Among all of the initial-guess configurations (Fig. S2), a few representative ones are shown in Fig. 1. The relevant bond lengths and adsorption energies are listed in Table 1. As shown in Fig. 1, for configuration **M1**, the double bound oxygen is directly coordinated to a surface five-coordinated Ti_{5c} atom, allowing the hydroxyl group to form a hydrogen bond with a double-coordinated surface O_{2c} atom. The calculated adsorption energy for **M1** is -0.89 eV. In Configuration **M2**, the hydroxyl group donates a proton to the nearest surface O_{2c} atom at a different row, and then the deprotonated O atom is bonded to a Ti_{5c} atom. The double bound O atom is not bonded to a Ti_{5c} atom but forms a hydrogen bond with the dissociated proton. In regard to **M3**, the hydroxamate is bonded to the TiO_2 surface by the Ti-N bond. The dissociated proton is transferred to the neighboring double bound oxygen, thus two hydroxyl groups can exist in configuration **M3**. Furthermore, we find that the protons of two hydroxyl groups remain hydrogen-bonded to the surface O_{2c} atoms, with distances d(O_{2c}-H) of 1.582 Å

and 1.752 Å, stabilizing the structure and producing an adsorption energy of -0.68 eV.

Configuration **B1** is a doubly deprotonated structure, with the double bound O atom and the deprotonated O atom coordinated to two different Ti_{5c} atoms, which leads to an adsorption energy of -0.67 eV. The dissociated protons in **B1** are, respectively, placed on nearby O_{2c} atoms. Configuration **B2** is also characterized by the dissociation of the N-H bond, with the dissociated proton placed on the nearest O_{2c} which belongs to a different row. In configuration **B2**, the double bound O atom and the deprotonated N atom are coordinated to different Ti_{5c} atoms, forming the bidentate bridging geometry. For this case, d(O_{2c}-H) is about 2.4 Å, indicating that the hydroxyl is involved neither in the surface bonding to Ti_{5c} atom nor in the formation of hydrogen bond to surface O_{2c} atom. Also, since it provides the worst adsorption energy, -0.53 eV, we will not discuss this configuration in the following. As for the last configuration, **B3**, differently from the cases of **B1** and **B2**, the dissociated proton comes from the hydroxyl group, with the double bound O atom and deprotonated O atom coordinated to different Ti_{5c} atoms, see Fig. 1. Its calculated adsorption energy is -0.89 eV.

Table 1. The calculated adsorption energies (in eV) and corresponding bond lengths (in Å).

	M1	**M2**	**M3**	**B1**	**B2**	**B3**
E_{ads}	-0.89	-0.81	-0.68	-0.67	-0.53	-0.89
d(Ti-O)$_1$	2.093	1.920	—	1.968	2.019	2.086
d(Ti-O)$_2$	—	—	—	1.837	—	1.959
d(Ti-N)	—	—	2.284	—	2.160	—
d(O_{2c}-H)$_1$	1.729	1.509	1.752	—	2.373	—
d(O_{2c}-H)$_2$	—	—	1.582	—	—	—

In order to explore the dynamics stability for configurations **M1**, **M2**, **M3**, **B1**, and **B3**, molecular dynamics simulations of these configurations were performed at 300 K. We present the time evolution of anchor bond lengths for some representative configurations in Fig. 2. First we note that all the Ti-O bonds in **M1**, **M2**, and **B1** are found to be stable, oscillating around their equilibrium values during the entire 4 ps trajectory. Conversely, the formed hydrogen bonds in **M1** and **M2** cannot maintain their stability during the trajectory. For example, in **M1**, the H-O bond vibrates around ~1.8 Å with a small amplitude of approximately 0.3 Å during the first 1.9 ps, then the H atom moves with a large amplitude (about 2 ~ 4 Å) relative to the O atom for the later 2.1 ps. We also verified that the molecule rotates and bends largely in the cases **M1** and **M2**. A similar behaviour occurs for configuration **M3**, as shown in Fig. S3. In the case of **B3**, one of its Ti-O bonds does not remain stable with respect to the other after the 3 ps time propagation. Overall, **B1** is the most kinetically stable configuration concerning the hydroxamate anchoring on the TiO_2 surface.

The vibrational spectra of the adsorbed (configuration **B1**) and free hydroxamic acid have been investigated at the DFT/B3LYP/6-31G(d) level of theory with the Gaussian 09[8]. The corresponding results are listed in Fig. S4 and Table S1. Previously, McQuillan et al. conducted an infrared spectroscopic study of acetohydroxamate acid adsorbed on titanium dioxide.[9] Noting that only the anchor group is shared between the acetohydroxamate acid in McQuillan's study[9] and the molecule of the present work, only those vibrations related to the anchor group have been considered. According our calculated results, the DFT-calculated vibrational frequencies for configuration **B1** agree generally with the experimental data, taking into account that discrepancies are expected due to differences between the substituent of hydroxamate, regarding theory (pyridine) and experiment (methyl). In particular, for the free anchor we observe a strong peak at about 1746 cm^{-1} which can be assigned to the C=O stretching mode, although it is weakened and further redshifted to 1651 cm^{-1} upon adsorption onto TiO_2 surface. This redshift is consistent with the experimental observation[9], indicating that carbonyl may be involved in the binding to the surface Ti_{5c}. Secondly, as shown in Fig. S4c, there is a prominent peak at 1425 cm^{-1} which is ascribed to the N-H and O-H bending modes, and it is shifted to the lower wavenumber of 1355 cm^{-1} upon adsorption, which can be assigned to the C-N and C=O as well as C-C stretching modes. Furthermore, a strong peak at around 823 cm^{-1} is shown in Fig. S4b but is almost absent for Fig. S4c. This mode can be assigned to the O_{2c}-H bending, which is probably related to the dissociation of N-H and O-H bonds and the protons placed on the surface O_{2c} atoms during the adsorption process. The similar behaviour has also occurred in the experiment, although it did not report on the wavenumber below 1000 cm^{-1}.

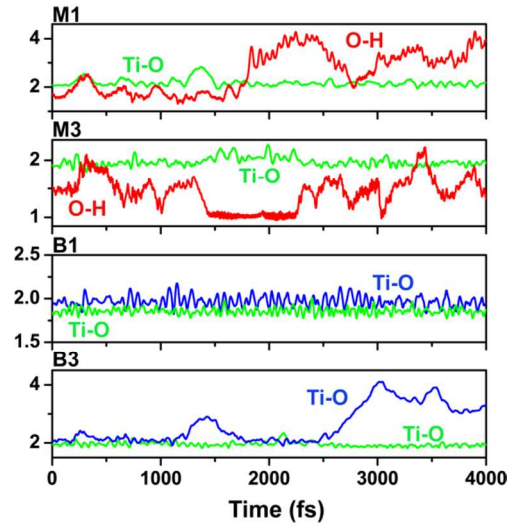

Fig. 2. Evolution of anchoring bond lengths in configurations **M1**, **M2**, **B1**, and **B3**

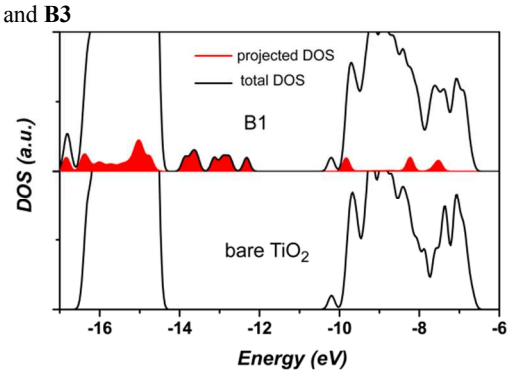

Fig. 3. Total and projected densities of states (DOS) calculated by the extended Hückel method for **B1** and a bare TiO_2 nanostructure

The density of states of the combined adsorbate/TiO_2 system were obtained by the semiempirical Extended-Hückel (EH) molecular orbital method. The detailed description of this methodology can be found in the supplementary information and elsewhere[10]. Fig. 3 presents the total and projected densities of states (DOS) of **B1** calculated by the EH method, as compared to the DOS of the bare TiO_2 nanostructure. The EH method predicts a band gap of about 4 eV for the $(TiO_2)_{32}$ model which is slightly larger than the experimental value of 3.4 eV for 2.4 nm particle.[10a] In general, the band gap for small TiO_2 clusters is overestimated with respect to the larger systems.[10b] The filled red curve represents the projected DOS onto electronic states of the adsorbate. It is shown that there are several virtual orbitals of the adsorbate, such as LUMO, LUMO+1, and LUMO+2, positioned within the TiO_2 conduction band in the range from -11 ~ -6 eV. These virtual molecular orbitals overlap in energy with electronic states of the TiO_2 conduction band, which is

suitable for interfacial electron injection. We show, in Fig. S5, some representative lowest unoccupied molecular orbitals. For comparison, the corresponding Kohn-Sham (KS) orbitals obtained at the DFT/B3LYP/6-31G(d) level are also included in Fig. S5. The semi-empirical calculations for the molecular orbitals are in excellent agreement with the corresponding ab initio calculations. In addition, both LUMO and LUMO+2 have significant electron population on the hydroxamate anchor. Conversely, for the LUMO+1, there is no electron occupation on the anchor group, which accounts for the slower interfacial electron injection from this orbital. Although several electronic states of adsorbate can be photo-excited, we concentrate our description on the LUMO orbital as the initial state for the following electron wavepacket propagation.

Next we analyse the interfacial electron transfer (IET) by means of quantum dynamics simulation. The quantum mechanical part of the method is based on a tight binding model Hamiltonian originates from the EH method. First of all, it has to be recognized that the presence of the hole influences the electron injection, since the electron-hole coupling could delay the electron transfer. But in most instances, the hole remains confined to the donor part of the adsorbate while the electron is injected. Therefore, for ultrafast interfacial electron transfer processes such as those studied herein, it is a good approximation to assume a static hole and just propagate the electronic wavepacket.[10b] The Coulomb coupling of the photo-excited electron and hole pair is described within the time-dependent Hartree approximation. The procedure for quantum propagation of the photo-excited electron is summarized in the supplementary information. $P(t)$ is the survival probability for the photo-excited electron to be in the adsorbate molecule at time *t* after the excitation of the system.

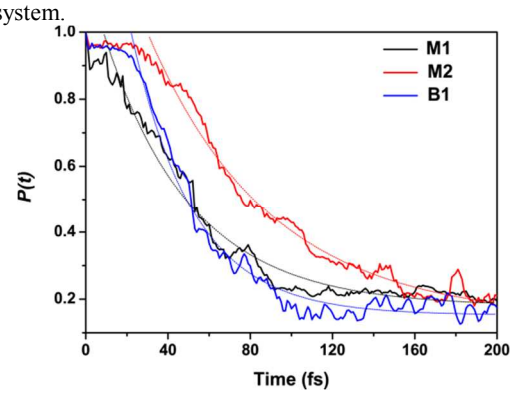

Fig. 4. Survival probability curves for electron injection starting from the adsorbate LUMO orbital of hydroxamate.

Fig. 4 shows the results for the survival probability $P(t)$ for M1, M2, and B1. Starting from the LUMO, it can be seen that the electron gradually delocalizes and is injected into the semiconductor region within the 200 fs time scale. Specifically, for **B1**, the electron is located at the adsorbate at the initial time (t = 0), then it begins to be rapidly injected after around t = 22 fs and finally evolves into stable oscillations after t = 93 fs. We show the representative snapshots of the time-dependent charge distribution in Fig. S6. The IET curve for **B1** can be well fitted by a decaying exponential function: $P(t) = 1.763\exp(-(t-22)/30.125) + 0.153$ for $t \geq 22$ fs. For **B1**, we find that the electron undergoes an ultrafast electron transfer from the adsorbate LUMO to the TiO_2 conduction band within a time scale of 53 fs with 31 fs decay time after a 22 fs delay. The ultrafast electron injection is more evident if we compare the electron density distribution for t = 0 fs with t = 53 fs, in Fig. 4. Following the same analysis we find that **M1** has the similar IET time scale of 53 fs. While for **M2**, it has the slower electron injection time scale of 92 fs compared with **B1** and **M1**, indicating that configurations **B1** and **M1** shall facilitate the faster electron injection process. In addition, the small survival population *P(t)* that remains for t > 100 fs can be ascribed to finite-size effects produced by the limited $(TiO_2)_{32}$ cluster model.

In conclusion, our theoretical results indicate that the bidentate bridging mode with the double-bonded O atom and deprotonated O atom coordinated to different Ti_{5c} atoms is the more dynamically stable configuration, and that the corresponding vibrational spectrum agrees with results of infrared spectroscopy experiment. Interfacial electron injection simulations suggest that this type of configuration yields an ultrafast electron injection, with a time scale of 53 fs. Overall, this work highlights the optimal adsorption mode for hydroxamic anchor, which is expected to provide valuable hints into the design of efficient anchor group for DSSC application.

This work was supported by the Natural Science Foundation of China (Grant No. 21003057, 21303068 and 21173096) and the State Key Development Program for Basic Research of China (Grant No. 2013CB834801) and Specialized Research Fund for the Doctoral Program of Higher Education (Grant No. 20110061110018).

Notes and references

[a] State Key Laboratory of Theoretical and Computational Chemistry, Institute of Theoretical Chemistry, Jilin University, Changchun 130023, People's Republic of China.

[b] Department of Physics, Universidade Federal de Santa Catarina, Florianópolis, SC 88040-900, Brazil.

E-mails: baifq@jlu.edu.cn; zhanghx@mail.jlu.edu.cn

Electronic Supplementary Information (ESI) available: additional figures and table as well as relevant theoretical backgrounds for the simulation of quantum dynamics. See DOI: 10.1039/c000000x

1 B. O'Regan, M. Grätzel, *Nature* **1991,** *353*, 737.

2 A. Yella, H. W. Lee, H. N. Tsao, C. Y. Yi, A. K. Chandiran, *Science* **2011,** *334*, 1203.

3 (a) B. Bozic-Weber, E. C. Constable, S. O. Furer, C. E. Housecroft, L. J. Troxler, J. A. Zampese, *Chem. Commun.* **2013**, doi: 10.1039/c3cc44595j; (b) K. R. Mulhern, A. Orchard, D. F. Watson, M. R. Detty, *Langmuir* **2012,** *28*, 7071

4 J. Warnan, L. Favereau, Y. Pellegrin, E. Blart, D. Jacquemin, F. A. Odobel, *J. Photoch. Photobio. A* **2011,** *226*, 9.

5 (a) T. P. Brewster, S. J. Konezny, S. W. Sheehan, L. A. Martini, C. A. Schmuttenmaer, V. S. Batista, R. H. Crabtree, *Inorg. Chem.* **2013,** *52*, 6752; (b) W. R. McNamara, R. L. Milot; H.-E. Song, R. C. Snoeberger III, V. S. Batista, C. A. Schmuttenmaer, G. W. Brudvig, R. H. Crabtree, *Energ. Environ. Sci.* **2010,** *3*, 917.

6 (a) G. Kresse, J. Furthmüllerb, *Comput. Mat. Sci.* **1996,** *6*, 15; (b) G. Kresse, J. Hafner, *Phys. Rev. B* **1994,** *49*, 14251; (c) G. Kresse, J. Hafner, *Phys. Rev. B* **1993,** *47*, 558; (d) G. Kresse, J. Furthmüllerb, *Phys. Rev. B* **1996,** *54*, 11169.

7 (a) J. P. Perdew, J. A. Chevary, S. H. Vosko, K. A. Jackson, M. R. Pederson, D. J. Singh, C. Fiolhais, *Phys. Rev. B* **1992,** *46*, 6671; (b) J. P. Perdew, J. A. Chevary, S. H. Vosko, K. A. Jackson, M. R. Pederson, D. J. Singh, C. Fiolhais, *Phys. Rev. B* **1993,** *48*, 4978.

8 Frisch et al. *Gaussian 09*, Revision D.01; Gaussian Inc.: Wallingford CT, 2009.

9 J. Yang, P. J. Bremer, L. L. Lamout, A. J. McQuillan, *Langmuir* **2006,** *22*, 10109.

10 (a) L. G. C. Rego, V. S. Batista, *J. Am. Chem. Soc.* **2003,** *125*, 7989; (b) D. A. Hoff, R. Silva, L. G. C Rego, *J. Phys. Chem. C* **2011,** *115*, 15617.